The Seismic Record
A journal of the Seismological Society of America

Raspberry Shake Instruments Provide Initial Ground-Motion Assessment of the Induced Seismicity at the United Downs Deep Geothermal Power Project in Cornwall, United Kingdom

Joanna M. Holmgren*[1] and Maximilian J. Werner[1]

Abstract

Raspberry Shake (RS) seismographs offer the potential for affordable and citizen-led seismic monitoring in areas with few publicly available seismometers, especially in previously quiescent regions experiencing induced seismicity. However, their scientific and regulatory potential remains largely untested. We examine the ground motions recorded by 11 RS and one broadband station within 15 km of the United Downs Deep Geothermal Power (UDDGP) project in Cornwall, United Kingdom, to evaluate the RS network's suitability to provide an initial ground-motion assessment of the region. To date, the British Geological Survey (BGS) has reported 232 induced events originating at UDDGP since flow testing began in summer 2020, with two events exceeding local magnitude (M_L) 1.5. Although the RS accelerometers are too noisy for UDDGP's microseismic events, the vertical geophones are useful. Peak ground velocity observations are consistent with relevant ground-motion models, whereas peak ground acceleration (PGA) values are greater than predicted. Regional trends in the PGA levels are likely caused by path effects. Finally, RS estimates of M_L are similar to those reported by the BGS. For sparse national seismic networks, RS stations can enable a preliminary evaluation of seismic events and their ground motions.

Cite this article as Holmgren, J. M. and Werner, M. J. (2021). Raspberry Shake Instruments Provide Initial Ground-Motion Assessment of the Induced Seismicity at the United Downs Deep Geothermal Power Project in Cornwall, United Kingdom. *The Seismic Record*. **1**, 27–34, doi: 10.1785/0320210010.

Introduction

With its low carbon footprint, geothermal energy is a promising alternative resource to hydrocarbons, but its development has been hampered by induced seismic risks. Although small microseismic events can be a natural and common occurrence at geothermal sites, a few recent cases of larger earthquakes have alarmed the public, caused damage, and paused or halted energy development, such as in Pohang, South Korea (Kim *et al.*, 2018) and Basel, Switzerland (Deichmann and Giardini, 2009). Knowledge of a region's expected ground motions is key to understanding the seismic hazards associated with geothermal energy production. Thus, early microseismic events can provide an initial determination of the appropriateness of the ground-motion models (GMMs) used for the site's planning and also reveal any unexpected regional trends in observed ground motions. In 2018, development of the United Downs Deep Geothermal Power (UDDGP) project started in Cornwall, southwest England (Ledingham *et al.*, 2019). UDDGP targets a fault zone in the Carnmenellis granitic pluton, utilizing the natural fracture permeability and gravity to circulate water between two wells drilled to 2.5 and 4.5 km depths (Paulillo *et al.*, 2020). Since flow testing began in summer 2020, 232 induced microseismic events in the previously quiescent region have been recorded by the British

1. School of Earth Sciences, University of Bristol, Bristol, United Kingdom, https://orcid.org/0000-0002-3371-8217 (JMH); https://orcid.org/0000-0002-2430-2631 (MJW)

*Corresponding author: joanna.holmgren@bristol.ac.uk

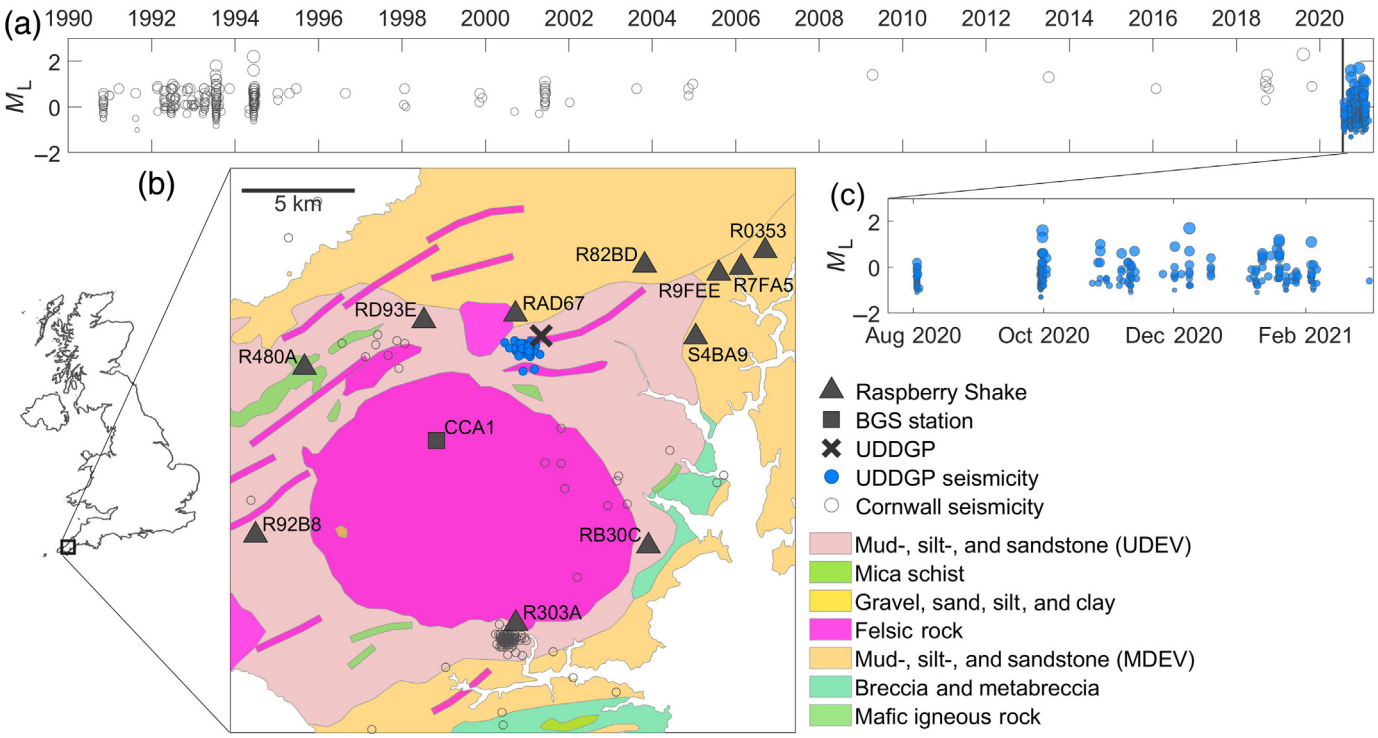

Figure 1. (a) Seismicity in Cornwall since 1990 in local magnitude (M_L). The seismicity linked to United Downs Deep Geothermal Project (UDDGP) is shaded blue. (b) Overview map of the United Kingdom and zoom-in of the Cornish region, with UDDGP (x), Raspberry stations (triangles), British Geological Survey (BGS) broadband (square), and seismicity (circles) indicated. Color coding denotes geology. MDEV and UDEV refer to Middle and Upper Devonian, respectively. (c) Zoom-in of the UDDGP seismicity timeline. The geological map is obtained from BGS (see Data and Resources). The earthquake clusters occurring 1990–1994 and in 2001 in panel (a) and located near R303A in panel (b) belong to the natural Constantine swarm (Walker and Browitt, 1994).

Geological Survey (BGS) (as of March 2021) (see Fig. 1). Although no ground motions have exceeded the site's "caution" peak ground velocity (PGV) level of 0.5 mm/s (UDDGP information sheet, see Data and Resources), two events have exceeded local magnitude (M_L) 1.5, providing sufficient data to conduct an initial review of the region's ground motions and to evaluate the suitability of relevant GMMs.

At present, there is only one public station from the national seismic network within 90 km of the UDDGP site, limiting the amount of available data to analyze the seismic hazard. Although both the BGS and the UDDGP operators, Geothermal Engineering Ltd. (GEL), have deployed local networks to monitor the induced seismicity, at the time of writing, the waveforms are not yet publicly available. However, GEL has provided near-by schools with seven Raspberry Shake (RS) stations in an effort to involve the surrounding communities in the geothermal project (H. Farndale, GEL, personal comm., 2021). Along with five RS deployed by hobbyists, 12 publicly available seismic stations are within 15 km of the site (Fig. 1). RSs are an affordable alternative to the more established and expensive seismic instruments available today (e.g., Anthony *et al.*, 2019), but their suitability for seismic hazard assessment of induced seismicity for scientific and regulatory purposes has not yet been examined. In western Nepal, Subedi *et al.* (2020) initiated a project to raise awareness of the region's seismic hazard by distributing RS instruments to schools and educating the local population about earthquake preparedness. During the first six months of installation in 2019, the RS network successfully recorded local earthquakes between M_L 4.0 and 5.2, and an RS scale relating PGV to M_L was developed. RSs have also successfully been used in combination with broadband sensors throughout the world to examine global seismic noise quieting due to COVID-19 lockdown measures (Lecocq *et al.*, 2020). In Cornwall, two different types of RS instruments are deployed: RS1D containing one vertical geophone, and RS4D containing one vertical geophone and three orthogonal accelerometers. Anthony *et al.* (2019) tested three RS4D in the laboratory to investigate the instrument response. They found that although the RS performed acceptably in terms of timing errors, the

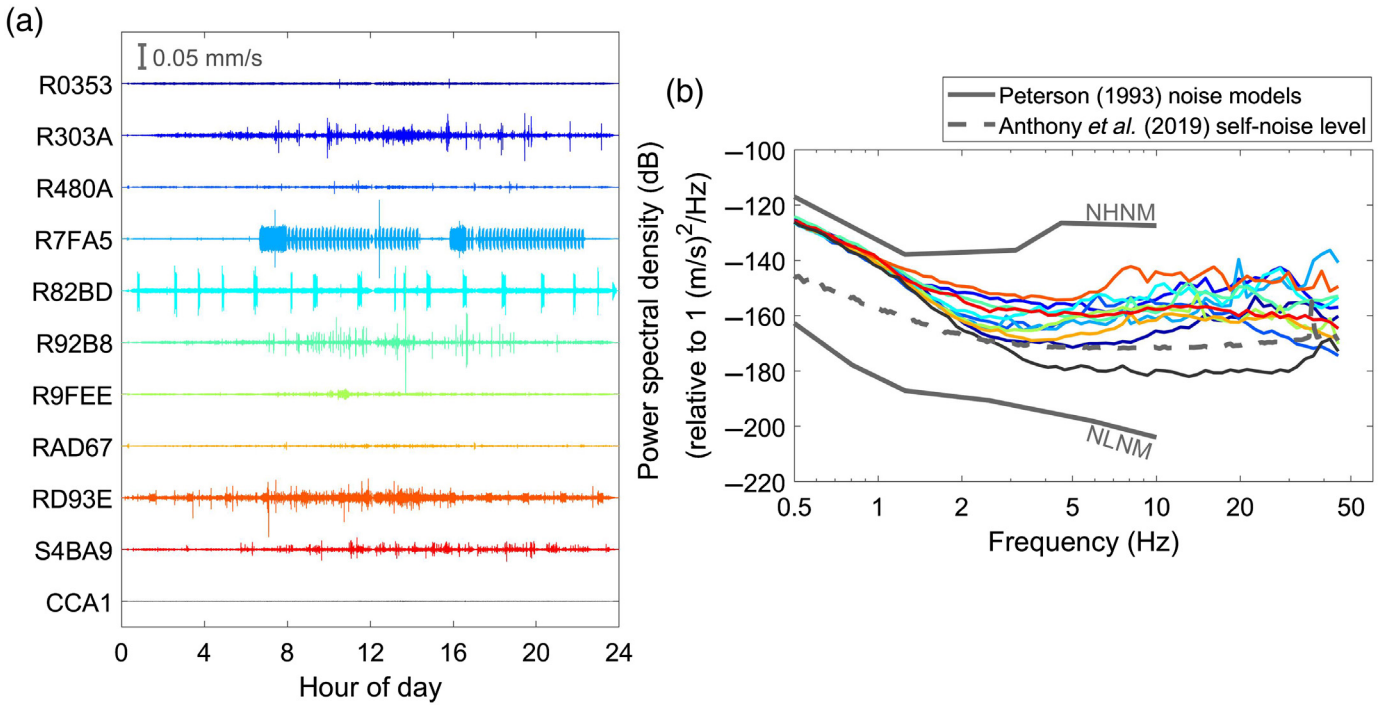

Figure 2. Noise analysis of a quiescent 24 hr day (14 November 2020). (a) Vertical ground velocity time series for the Raspberry Shake (RS, colored traces) and BGS broadband station (CCA1, black trace). All traces are high-pass filtered (1 Hz) and scaled equally in amplitude for comparability. (b) Averaged velocity power spectral density (PSD) for each station using 50% overlapping 1 hr time windows of the waveforms in panel (a) and color coded as in panel (a). The Peterson (1993) new high-noise model (NHNM) and new low-noise model (NLNM) are shown as a reference, along with the RS4D geophone self-noise curve from Anthony *et al.* (2019).

largest limitation was the sensors' high self-noise levels, especially those of the accelerometers. They determined that the strong-motion instruments are more suitable for recording large (magnitude > 6) local earthquakes.

Here, we investigate the ground motions recorded by the Cornwall RS network to assess its suitability in the (present) absence of data from a traditional seismic network. To assess the network's usability and limitations, we investigate noise levels, calculate observed PGV and peak ground acceleration (PGA), evaluate GMMs, and finally estimate M_L to find the magnitude of completeness and compare to the BGS M_L.

UDDGP Induced Seismicity and Publicly Available Stations

Since August 2020, the BGS has reported 232 induced earthquakes originating at the UDDGP site, spanning local magnitudes (M_L) between −1.3 and 1.7 and depths between 4.1 and 5.2 km (see Data and Resources). The locations and magnitudes are estimated by the BGS, using triggered event data provided by GEL's monitoring network. At present, there are 12 publicly available stations within 15 km of the site: two RS1Ds, nine RS4Ds, and one broadband seismometer from the BGS national seismic network (Fig. 1b). Most of the RS stations are located on sedimentary rocks originating from the Devonian period, whereas the broadband and one of the RS stations are located on the granitic intrusion (BGS, see Data and Resources). The closest RS station (RAD67) is 1.4 km away (epicentral distance) from the site, and the BGS broadband (CCA1) is 6.6 km away. The combination of high noise levels and the events' low magnitudes made the accelerometers unusable, limiting the study to only the vertical geophones. The geophones contain a single-component 4.5 Hz sensor with an electronic extension allowing usable frequencies down to ~1 Hz, with a 100 Hz sampling frequency. The broadband seismometer is a 100 Hz Nanometrics Trillium (240 s natural period).

As an initial evaluation of the stations, we pick a quiescent 24 hr period when most of the instruments were active to analyze the noise levels (Fig. 2). The availability of the RS varied from station to station, most experiencing periods when they were temporarily turned off. RB30C was only active until the beginning of October 2020 and is not included in Figure 2. We first assess temporal trends of the stations' time series by instrument

correcting and scaling them to make their amplitudes comparable (Fig. 2a). We also evaluate each station's power spectral density (PSD) function by splitting the instrument-corrected traces into 50% overlapping 1 hr segments, computing the PSD using multitaper (Prieto *et al.*, 2009), and finding the average over the 24 hr period (Fig. 2b). As reference, we include the Peterson (1993) new high- and low-noise models , and the RS4D geophone self-noise curve from Anthony *et al.* (2019). As expected, the BGS broadband station (CCA1, black line) has the lowest noise level, seen both by the low relative amplitude in its time series and the PSD. The RS stations, on the other hand, experience various types of noise over the duration of the day. We observe similar trends for each station in all 24 hr segments that we investigated. The higher noise levels in the RS instruments are likely due to a combination of deployment in suboptimal locations near anthropogenic noise, such as machinery in buildings or train tracks, and the high self-noise levels (Anthony *et al.*, 2019).

Ground-Motion Analysis

We estimate PGV and PGA of the vertical components for all earthquakes using the RS and broadband instruments to evaluate their suitability as an alternative to more established seismic networks. First, we analyze the signal-to-noise ratio (SNR) of the events in the frequency domain by selecting 6 s time windows encompassing the *P*, *S*, and coda waves and pre-*P*-wave noise windows of equal length. We remove any events with SNR below 2. The instrument-corrected time series are then filtered around the good SNR bandwidth using a two-pole, two-pass Butterworth filter and differentiated to retrieve acceleration time series. To ensure sufficient frequency coverage for usable PGV and PGA measurements, we denote f_1 and f_2 as the minimum and maximum acceptable SNR frequencies, respectively, and evaluate their coverage. PGV is generally related to the moderate frequencies, whereas PGA reflects the higher frequencies (Booth, 2007). Here, we require $f_2/f_1 \geq 2$ and $2f_1 \leq 10$ Hz to compute PGV (Edwards *et al.*, 2021), and $f_2 \geq 35$ Hz for a usable PGA measurement. To remove any records due to noise peaks, we only keep events recorded on either the broadband station (CCA1) or the closest and relatively quiet RS station (RAD67). Any extreme outliers were manually examined to see if they were noise or earthquake and removed accordingly. This resulted in 225 PGV observations for 85 events and 198 PGA observations for 83 events, spanning M_L between −1.1 and 1.7.

In ground-motion analysis, moment magnitude (M_w) is the preferred magnitude scale. Because BGS reports in M_L, we use the Butcher *et al.* (2020) conversion developed for small earthquakes in New Ollerton, United Kingdom:

$$M_w = 0.69M_L + 0.74. \quad (1)$$

This leads to M_w between 0.0 and 1.9.

Figure 3 shows the observed PGV and PGA values plotted against hypocentral distance. The average event depth is 4.8 km. As a reference, PGV thresholds have been included for the UDDGP cautious state at 0.5 mm/s, when humans can detect motion at 2.0 mm/s, and when UDDGP takes action at 8.5 mm/s (GEL information sheet, see Data and Resources). We also examine the two largest events (M_L 1.6 and 1.7, or equivalently M_w 1.84 and 1.91, shaded dark-gray circles and squares in Fig. 3) and compare their PGA and PGV observations to three relevant GMMs. Douglas *et al.* (2013; hereafter, D13) developed a GMM for geothermally induced seismicity from Europe and United States, uncorrected for site, and targeting $M_w \geq 1$ and hypocentral distances (R_{hypo}) < 30 km. Cremen *et al.* (2020; hereafter, C20) adjusted the Douglas GMM to create a model for $M_L \geq 0$ and $R_{hypo} \leq 10$ km, using induced events from a shale gas site (Preston New Road) and a coal mining site in the United Kingdom. Finally, Edwards *et al.* (2021; hereafter, E21) adjusted the Atkinson (2015) induced seismicity GMM using the Preston New Road dataset to target $M_L \geq 0.25$ and $R_{hypo} < 25$ km. We note that all three GMMs are developed for horizontal ground motions. Preferably, the vertical RS ground motions should be converted to their horizontal counterpart or the GMMs to their vertical counterpart. However, because this conversion factor is unknown for the RS and GMMs, we assume that the vertical and horizontal are equal.

As can be seen in Figure 3a, the PGV observations of the two largest events are adequately predicted by the D13 GMM, although higher than expected by the C20 and E21 models. Interestingly, the PGA observations are higher than predicted by all three models (Fig. 3b). The discrepancies could be due to several reasons. One reason could be that the region simply experiences more high-frequency content than other regions, caused by higher earthquake stress drops or alternatively less path and site attenuation. This would imply that the UDDGP site should not rely on these three GMMs for their seismic hazard assessments, and that they need a GMM adjusted specifically for Cornwall to predict the ground-motion levels adequately. Another reason for the discrepancies could be linked to our (necessary) usage of the vertical component, whereas the GMMs model horizontal ground motions. In

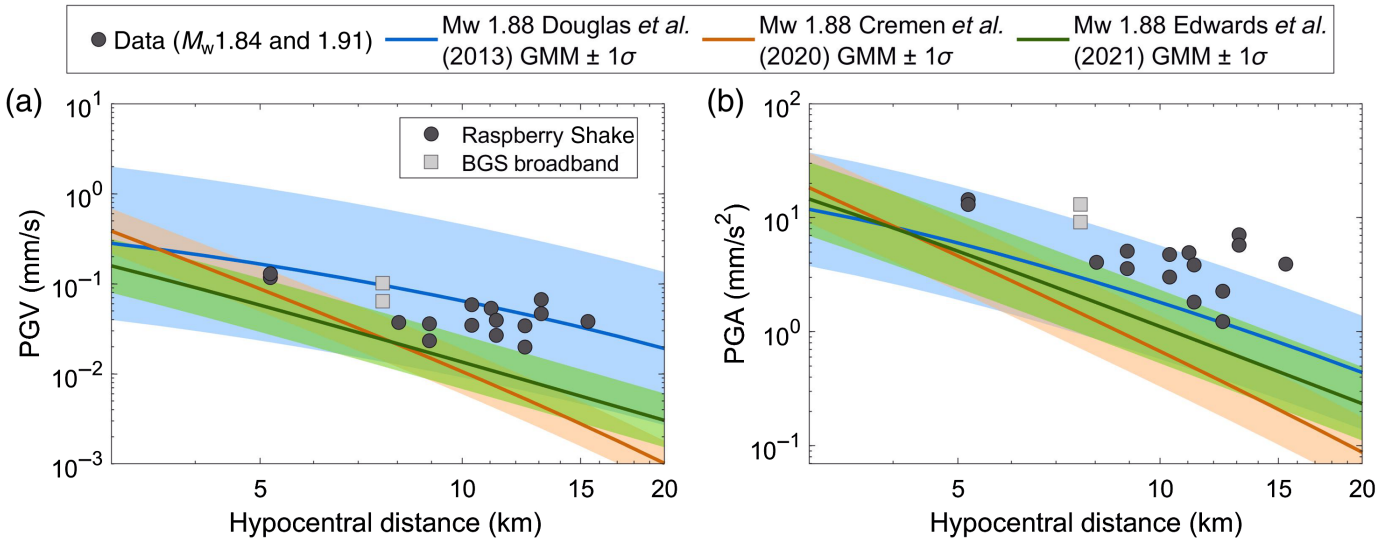

Figure 3. (a) Peak ground velocity (PGV) and (b) peak ground acceleration (PGA) observations of the UDDGP seismicity. The average event depth is 4.8 km. RS observations are shown as circles and BGS broadband as squares. The two largest induced events from UDDGP (M_w 1.84 and 1.91) are shaded dark gray. Three ground-motion models (GMMs) for an M_w 1.88 event are shown as solid lines, with the shaded areas representing $\pm 1\sigma$. PGV thresholds at 0.5 mm/s when UDDGP enters "cautious" state, 2.0 mm/s when humans can detect ground motion, and 8.5 mm/s when UDDGP takes action have been included as a reference in panel (a).

general, the horizontal component includes more site characteristics than the vertical (Lermo and Chávez-García, 1993). The D13 GMM does not include site effects, plausibly explaining the better match with PGV values, whereas both the C20 and E21 GMMs are adjusted to the shale gas environments they were developed for. Finally, the events' M_w are not estimated from the data directly, but instead estimated using an empirical scale developed for a coal mine environment (equation 1, Butcher *et al.*, 2020). Thus, there will be differences in the path and site effects compared to a geothermal site targeting a granite, which could result in M_w and GMM-level discrepancies.

To further evaluate the RS ground motions, we estimate station terms using the PGA observations. We choose PGA because it reflects the high-frequency content of earthquakes and site parameters, such as κ and f_{max}, primarily affect the higher frequencies. Using the E21 GMM, we compute PGA intraevent residuals for all $M_L \geq 0.25$ earthquakes. E21 was developed for similar earthquake sizes and distances to the UDDGP dataset, while having a smaller sigma (σ) than D13. Intraevent residuals reflect the record-to-record variability caused by site and path effects not encompassed by the GMM (Atik *et al.*, 2010). Figure 4a shows the intraevent residuals against distance, highlighted in the corresponding geological color. Each station's median intraevent residual is shown in Figure 4b, grouped according to lithology. Both the smallest and largest residuals, indicating lower and higher observed PGA than expected, respectively, correspond to mud-, silt-, and sandstone stations. Thus, site effects are less likely the cause behind the station trends. One plausible explanation

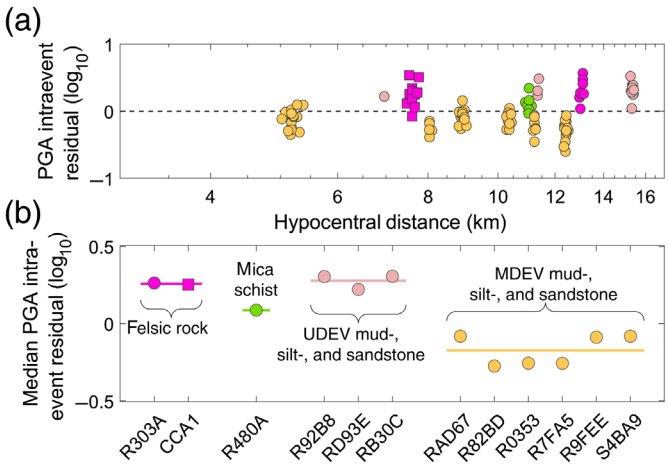

Figure 4. PGA intraevent residuals compared to geological setting, using the Edwards *et al.* (2021) GMM and $M_L \geq 0.25$. (a) Intraevent residuals plotted against hypocentral distance, color coded according to station geology (see Fig. 1). (b) Median station intraevent residuals grouped based on geology.

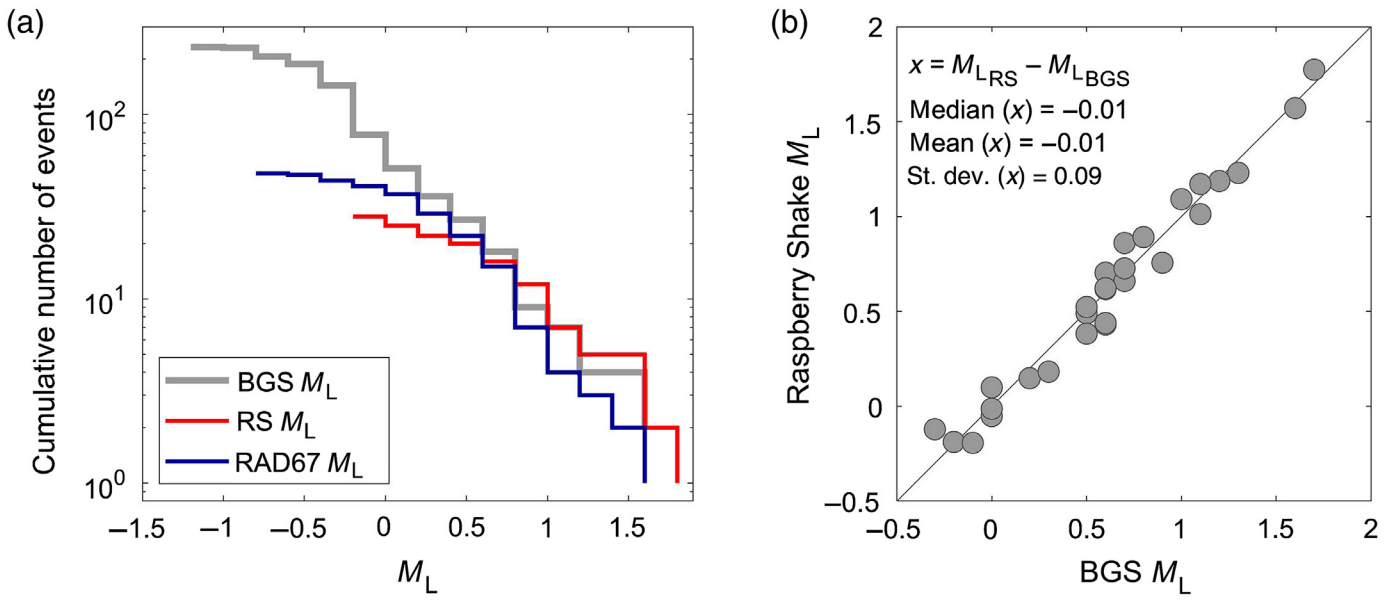

Figure 5. (a) Local magnitude (M_L) distribution using the BGS catalog, RS network, and closest RS station (RAD67, R_{hypo} = 5 km). (b) Comparison of M_L estimated by the BGS and by the RS instruments.

could be linked to the travel paths of the seismic waves. The UDDGP site is situated on the northeastern side of the Carnmenellis granitic pluton, which is on average 3–4 km deep and extends down to 23 km in the center (Taylor, 2007). The travel path between the UDDGP seismicity and the north-northeastern Middle Devonian mud-, silt-, and sandstone stations is mostly through sedimentary rocks (Fig. 1). In contrast, the seismic waves must travel through the granitic pluton for longer to reach the remaining stations. Because of granite's lower-attenuation properties, the ground motions at the remaining stations are less attenuated, resulting in larger amplitudes. Furthermore, the lithological alteration caused by the Carnmenellis pluton baking and stiffening its surrounding host rock could also lead to harder rock and lower-attenuation properties.

Local Magnitude Analysis

Traffic light systems commonly use PGV or M_L to monitor induced seismicity. As a final assessment of the RS stations, we estimate the M_L of the UDDGP events, excluding the BGS broadband seismometer. We use the M_L scale developed for the United Kingdom by Luckett *et al.* (2019) and currently used by the BGS:

$$M_L = \log_{10} A + 1.11 \log_{10}(R_{hypo}) + 0.00189 R_{hypo} - 1.16 e^{-0.2 R_{hypo}} - 2.09, \quad (2)$$

in which A is the largest zero-to-peak displacement amplitude in nanometers, and R_{hypo} is the hypocentral distance in kilometers. The term $-1.16e^{-0.2R_{hypo}}$ accounts for observations at close distances ($0 < R_{hypo} < 20$ km). We convert all instrument-corrected traces to Wood–Anderson seismographs, assuming that the response of a 1.25 Hz Wood–Anderson instrument with 0.8 damping can be approximated by a 2 Hz high-pass filter (Havskov and Ottemoller, 2010). Using a 6 s time window and removing records with SNR < 2, we compute the M_L for all RS stations. We then estimate each event M_L as the median of its stations' M_L, requiring a minimum of three station M_L per event, and obtain 28 event M_L ranging between −0.2 and 1.8. The reported BGS M_L were computed via equation (2) using horizontal data from the local GEL network (B. Baptie, BGS, personal comm., 2021).

Figure 5a compares the M_L distributions from the BGS catalog and RS stations. Unsurprisingly, the BGS M_L has the lowest magnitude of completeness (M_c) at ∼ − 0.4. A larger M_c of ∼0.8 is obtained from the RS network caused by high noise levels masking the smaller events. We also include the M_L distribution estimated by the closest RS station (RAD67, R_{hypo} = 5 km), located at similar distance as the GEL stations. Although RAD67's M_c (∼0.2) is still larger than the BGS M_c and estimated using only one station, it demonstrates that deploying more RS at closer distances could lower the M_c. A lower M_c can, for example, improve the b-value estimate

and provide more useful events for developing and testing forecast models.

Finally, we compare the RS M_L to the M_L reported by the BGS (see Fig. 5b). Interestingly, the vertical RS geophones were able to predict similar M_L to the BGS, with a median difference of −0.01. Theoretically, the BGS M_L should be larger because the horizontal component is amplified at the site, unless the site is hard rock in which case the vertical and horizontal amplitudes are comparable (Alsaker *et al.*, 1991). Anthony *et al.* (2019) found that the higher self-noise of RS can lead to larger M_L for small events. To investigate this, we compared our RS M_L to the vertical broadband (CCA1) M_L and did not find RS M_L relatively larger than CCA1 M_L with decreasing magnitude. Another plausible explanation could be the distance correction factor in equation (2); considering the close proximity of the GEL network, these stations will have been more strongly corrected than the average RS station. Using the M_L equation without the additional near-field correction might have resulted in higher M_L for BGS.

Discussion and Conclusion

We have evaluated the performance of a network of private citizen-operated and affordable RS stations to record ground motions of induced microseismicity associated with flow testing at the UDDGP site. Notwithstanding data-quality challenges, the RS network can provide an initial determination of the applicability of GMMs and thus has significant potential for wider monitoring usage, seismic hazard assessment, and citizen–scientist involvement. Local magnitudes determined with the RS network also matched BGS magnitudes very closely. Another component to seismic monitoring is determining locations, which can be challenging without a detailed velocity model. In this study, we used the locations reported by the BGS. However, geothermal-induced seismicity tends to occur near the production well opening (e.g., Kwiatek *et al.*, 2019), providing an acceptable proxy location for an initial earthquake assessment if locations were not available.

Limitations of the RS sensors are, however, important to characterize. RS noise levels are high compared to the publicly available broadband in the region. In addition to the high self-noise of RS instruments (Anthony *et al.*, 2019), several of the stations were also exposed to high external noise levels, likely caused by the environments they were installed in. High noise levels are especially limiting when events are small and easily masked by interfering signals. Furthermore, permanent seismic networks rely on the quality and availability of their stations and are regularly maintained by technicians. The same level of technical support may not be available to private RS owners. The availability of the RS in Cornwall varied from station to station, but most stations had periods when they were turned off. To ensure a resilient network capable of continuous monitoring when individual stations are offline, RS networks thus need sufficiently many sensors.

Another limitation of the RS stations in this study was that only the vertical geophones were usable; because of their high noise levels, we had to discard all accelerometer data and instead assume that horizontal and vertical motions are equal. Generally, buildings are more vulnerable to horizontal motions, and thus the horizontal component is preferred for GMMs and M_L analysis. Nonetheless, the RS instruments provide a useful preliminary assessment of the ground motions associated with the induced seismicity at the UDDGP site. We were able to evaluate the suitability of different GMMs for the region, examine regional trends in the observed ground-motion levels likely due to a combination of site and path effects, and estimate M_L comparable to the BGS network. We conclude that an RS network is a suitable alternative for preliminary (but not definitive) seismic hazard analysis in regions lacking publicly available data from established seismic networks.

Data and Resources

The British Geological Survey (BGS) earthquake catalog for the United Downs Deep Geothermal Power (UDDGP) events is available through their database search at http://www.earthquakes.bgs.ac.uk/earthquakes/dataSearch.html (last accessed March 2021). The BGS geological map of Cornwall is obtained from https://ngdc.nerc.ac.uk/products/digitalmaps/dataInfo.html (last accessed February 2021). The Raspberry Shake data are available through the Raspberry Shake International Federation of Digital Seismograph Networks (FDSN) server (http://www.fdsn.org/networks/detail/AM/, last accessed March 2021). The BGS data are available from the BGS FDSN server (https://eida.bgs.ac.uk/, last accessed March 2021). All waveforms were downloaded and instrument corrected using Obspy (Beyreuther *et al.*, 2010). Processing was carried out in MATLAB (www.mathworks.com/products/matlab, last accessed March 2021). The Geothermal Engineering Ltd. (GEL) UDDGP information sheet can be found at https://geothermalengineering.co.uk/wp-content/uploads/2020/08/Seismicity-Information-Sheet.pdf (last accessed February 2021).

Declaration of Competing Interests

The authors declare no competing interests.

Acknowledgments

The authors thank Reviewers Robert Anthony and John Douglas and Editor Keith Koper for their useful comments, which have helped improve this article. In addition, Brian Baptie, Anthony Butcher, Gemma Cremen, Jessica Irving, and Robert Myhill are thanked for their valuable help and discussion. Maximilian J. Werner would like to acknowledge Mark Vanstone's great Twitter feed (@wmvanstone) about seismology enabled by Raspberry Shakes. This research was supported by Natural Environment Research Council (NERC) (NE/R017956/1, "EQUIPT4RISK") and the Bristol University Microseismic ProjectS ("BUMPS").

References

Alsaker, A., L. B. Kvamme, R. A. Hansen, A. Dahle, and H. Bungum (1991). The M_L scale in Norway, *Bull. Seismol. Soc. Am.* **81,** no. 2, 379–398.

Anthony, R. E., A. T. Ringler, D. C. Wilson, and E. Wolin (2019). Do low-cost seismographs perform well enough for your network? An overview of laboratory tests and field observations of the OSOP Raspberry Shake 4D, *Seismol. Res. Lett.* **90,** no. 1, 219–228.

Atik, L. A., N. Abrahamson, J. J. Bommer, F. Scherbaum, F. Cotton, and N. Kuehn (2010). The variability of ground-motion prediction models and its components, *Seismol. Res. Lett.* **81,** no. 5, 794–801.

Atkinson, G. M. (2015). Ground-motion prediction equation for small-to-moderate events at short hypocentral distances, with application to induced-seismicity hazards, *Bull. Seismol. Soc. Am.* **105,** no. 2A, 981–992.

Beyreuther, M., R. Barsch, L. Krischer, T. Megies, Y. Behr, and J. Wassermann (2010). ObsPy: A Python toolbox for seismology, *Seismol. Res. Lett.* **81,** no. 3, 530–533.

Booth, E. (2007). The estimation of peak ground-motion parameters from spectral ordinates, *J. Earthq. Eng.* **11,** no. 1, 13–32.

Butcher, A., R. Luckett, M. J. Kendall, and B. Baptie (2020). Seismic magnitudes, corner frequencies, and microseismicity: Using ambient noise to correct for high-frequency attenuation, *Bull. Seismol. Soc. Am.* **110,** no. 3, 1260–1275.

Cremen, G., M. J. Werner, and B. Baptie (2020). A new procedure for evaluating ground-motion models, with application to hydraulic-fracture-induced seismicity in the United Kingdom, *Bull. Seismol. Soc. Am.* **110,** no. 5, 2380–2397.

Deichmann, N., and D. Giardini (2009). Earthquakes induced by the stimulation of an enhanced geothermal system below Basel (Switzerland), *Seismol. Res. Lett.* **80,** no. 5, 784–798.

Douglas, J., B. Edwards, V. Convertito, N. Sharma, A. Tramelli, D. Kraaijpoel, B. M. Cabrera, N. Maercklin, and C. Troise (2013). Predicting ground motion from induced earthquakes in geothermal areas, *Bull. Seismol. Soc. Am.* **103,** no. 3, 1875–1897.

Edwards, B., H. Crowley, R. Pinho, and J. J. Bommer (2021). Seismic hazard and risk due to induced earthquakes at a shale gas site, *Bull. Seismol. Soc. Am.* **111,** no. 2, 875–897, doi: 10.1785/0120200234.

Havskov, J., and L. Ottemoller (2010). *Routine Data Processing in Earthquake Seismology: With Sample Data, Exercises and Software*, Springer Science & Business Media, New York, New York, 347 pp.

Kim, K. H., J. H. Ree, Y. Kim, S. Kim, S. Y. Kang, and W. Seo (2018). Assessing whether the 2017 M_w 5.4 Pohang earthquake in South Korea was an induced event, *Science* **360,** no. 6392, 1007–1009.

Kwiatek, G., T. Saarno, T. Ader, F. Bluemle, M. Bohnhoff, M. Chendorain, G. Dresen, P. Heikkinen, I. Kullonen, P. Leary, *et al.* (2019). Controlling fluid-induced seismicity during a 6.1-km-deep geothermal stimulation in Finland, *Sci. Adv.* **5,** no. 5, eaav7224, doi: 10.1126/sciadv.aav7224.

Lecocq, T., S. P. Hicks, K. Van Noten, K. Van Wijk, P. Koelemeijer, R. S. De Plaen, F. Massin, G. Hillers, R. E. Anthony, M. T. Apoloner, *et al.* (2020). Global quieting of high-frequency seismic noise due to COVID-19 pandemic lockdown measures, *Science* **369,** no. 6509, 1338–1343.

Ledingham, P., L. Cotton, and R. Law (2019). The United Downs Deep Geothermal Power project, *Proc. 44th Workshop on Geothermal Reservoir Engineering*, 1–11.

Lermo, J., and F. J. Chávez-García (1993). Site effect evaluation using spectral ratios with only one station, *Bull. Seismol. Soc. Am.* **83,** no. 5, 1574–1594.

Luckett, R., L. Ottemöller, A. Butcher, and B. Baptie. (2019). Extending local magnitude M_L to short distances, *Geophys. J. Int.* **216,** no. 2, 1145–1156.

Paulillo, A., L. Cotton, R. Law, A. Striolo, and P. Lettieri (2020). Geothermal energy in the UK: The life-cycle environmental impacts of electricity production from the United Downs Deep Geothermal Power project, *J. Clean. Prod.* **249,** 119,410, doi: 10.1016/j.jclepro.2019.119410.

Peterson, J. R. (1993). Observations and modeling of seismic background noise, *U.S. Geol. Surv. Open-File Rept. 93-322*, 95 pp.

Prieto, G. A., R. L. Parker, and I. F. L. Vernon (2009). A Fortran 90 library for multitaper spectrum analysis, *Comput. Geosci.* **35,** no. 8, 1701–1710.

Subedi, S., G. Hetényi, P. Denton, and A. Sauron (2020). Seismology at school in Nepal: A program for educational and citizen seismology through a low-cost seismic network, *Front. Earth Sci.* **8,** 73.

Taylor, G. K. (2007). Pluton shapes in the Cornubian Batholith: New perspectives from gravity modelling, *J. Geol. Soc.* **164,** no. 3, 525–528.

Walker, A. B., and C. W. A. Browitt (1994). BGS seismic monitoring and information service fifth annual report, *British Geol. Surv. Tech. Rept. WL/94/10*, available at https://earthquakes.bgs.ac.uk/publications/annual_reports/1994_5th_annual_report.pdf (last accessed May 2021).

Manuscript received 31 March 2021
Published online 13 May 2021